AD-A156 993 A DIFFERENTIAL PREDICTION METHOD FOR THREE-DIMENSIONAL LAMINAR AND TURBUL..(U) DAVID W TAYLOR NAVAL SHIP RESEARCH AND DEVELOPMENT CENTER BET.. 1/1

UNCLASSIFIED N C GROVES ET AL. JUN 85 DTNSRDC-85/058 F/G 20/4 NL

END
DATE FILMED
8-85
DTIC

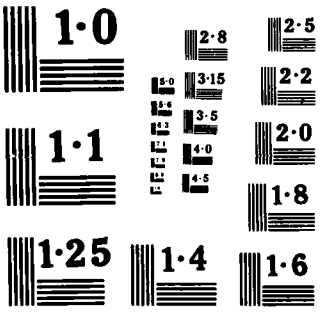
1·0
1·1
1·25
1·4
1·6
1·8
2·0
2·2
2·5
2·8
3·15
3·5
4·0
4·5
5·0

UNCLASSIFIED

SECURITY CLASSIFICATION OF THIS PAGE

REPORT DOCUMENTATION PAGE

1a REPORT SECURITY CLASSIFICATION UNCLASSIFIED	1b RESTRICTIVE MARKINGS
2a SECURITY CLASSIFICATION AUTHORITY	3 DISTRIBUTION / AVAILABILITY OF REPORT APPROVED FOR PUBLIC RELEASE; DISTRIBUTION IS UNLIMITED
2b DECLASSIFICATION / DOWNGRADING SCHEDULE	
4 PERFORMING ORGANIZATION REPORT NUMBER(S) DTNSRDC-85/058	5 MONITORING ORGANIZATION REPORT NUMBER(S)
6a NAME OF PERFORMING ORGANIZATION David W. Taylor Naval Ship R&D Center 6b OFFICE SYMBOL (If applicable) Code 1542	7a NAME OF MONITORING ORGANIZATION
6c ADDRESS (City, State, and ZIP Code) Bethesda, Maryland 20084-5000	7b ADDRESS (City, State, and ZIP Code)
8a NAME OF FUNDING / SPONSORING ORGANIZATION 8b OFFICE SYMBOL (If applicable)	9 PROCUREMENT INSTRUMENT IDENTIFICATION NUMBER
8c ADDRESS (City, State, and ZIP Code)	10 SOURCE OF FUNDING NUMBERS PROGRAM ELEMENT NO: 61152N; PROJECT NO:; TASK NO: ZR 0230101; WORK UNIT ACCESSION NO: DN 478002

11 TITLE (Include Security Classification)
A DIFFERENTIAL PREDICTION METHOD FOR THREE-DIMENSIONAL LAMINAR AND TURBULENT BOUNDARY LAYERS OF ROTATING PROPELLER BLADES

12 PERSONAL AUTHOR(S)
Nancy C. Groves and Ming-Shun Chang

13a TYPE OF REPORT	13b TIME COVERED	14 DATE OF REPORT (Year, Month, Day)	15 PAGE COUNT
Final	FROM _____ TO _____	1985 June	25

16 SUPPLEMENTARY NOTATION
Presented at the 15th ONR Symposium, Hamburg, Germany, 3-7 September 1984

17 COSATI CODES		
FIELD	GROUP	SUB-GROUP

18 SUBJECT TERMS (Continue on reverse if necessary and identify by block number)
Three-dimensional, boundary layer, propeller blades, laminar, turbulent, numerical calculation

19 ABSTRACT (Continue on reverse if necessary and identify by block number)

A general formulation is given for the three-dimensional boundary-layer flow on a rotating propeller blade. The basic equations are presented in a nonorthogonal coordinate system which rotates with the blade. Finite difference methods are used to develop a computer code for solving the laminar and turbulent boundary-layer equations. The Reynolds stress tensor is modeled by an algebraic eddy-viscosity formulation. In general, the equations are solved numerically using the standard Keller box method. However, regions of flow reversal across the boundary-layer are computed by the characteristic box method. A companion geometry computer code, developed to model propeller geometry characteristics, and an existing inviscid flow code for computing propeller blade pressures are combined with the boundary-layer computer code to form

(Continued on reverse side)

20 DISTRIBUTION / AVAILABILITY OF ABSTRACT	21 ABSTRACT SECURITY CLASSIFICATION
☒ UNCLASSIFIED/UNLIMITED ☐ SAME AS RPT ☐ DTIC USERS	UNCLASSIFIED
22a NAME OF RESPONSIBLE INDIVIDUAL Nancy C. Groves	22b TELEPHONE (Include Area Code) (202) 227-1605 22c OFFICE SYMBOL Code 1542

DD FORM 1473, 84 MAR 83 APR edition may be used until exhausted
All other editions are obsolete

SECURITY CLASSIFICATION OF THIS PAGE
UNCLASSIFIED

(Block 19 Continued)

an efficient computation scheme. For a given potential-flow solution, a typical boundary-layer solution of 690 grid points requires 64 seconds CPU time on a CYBER 176 computer.

Computed results are presented for several blade geometries. The rotating segment solution compares well with analytical and experimental data. Predictions for a model propeller also compare favorably with experimental data and illustrate that two-dimensional theory may provide adequate predictions for applications where crossflow effects are not important. Geometry effects of warp and skew are shown to be small for the boundary-layer predictions on three model propellers.

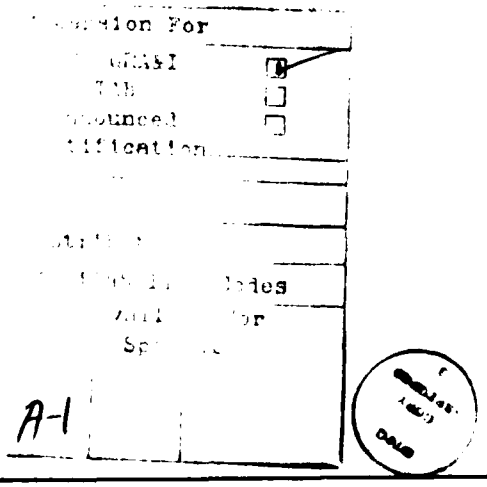

TABLE OF CONTENTS

LIST OF FIGURES

Page

NOTATION

A	Turbulence modeling damping factor
$C_{f\theta}$, C_{fr}	Streamwise and radial skin friction coefficients, respectively
f', g'	Nondimensional velocities, $f' = \frac{u}{u_e}$ and $g' = \frac{w}{u_{ref}}$
H	Shape factor
h_1, h_2, h_3	Metric coefficients for the ξ, η, and ζ coordinates, respectively
K_1, K_2	Geodesic curvatures of the curves η = constant and ξ = constant, see Eq. 4
K_{12}, K_{21}	Geometric parameters, see Eq. 5
L	Mixing length approximation
m_1 through m_{17}	Solution coefficient terms, see Eqs. 16 and 17
p	Static pressure in the fluid
R_n	Reynolds number at 0.7-radius, see Eq. 27
u, v, w	Velocity components in the ξ, ζ, and η directions, respectively
$\overline{u'v'}$, $\overline{v'w'}$	Reynolds stresses
u_{ref}	Reference velocity
x, y, z	Cartesian coordinate system where x is the axis of rotation (positive displacement measured aft), z is upward positive, and y forms a right-handed orthogonal system, see Figure 1
x_c	Fraction of chord, measured from leading edge
x_R	Nondimensional radius, fraction of tip radius
α	Angle between the ξ and η surface coordinates
β	Limiting streamline angle
δ	Boundary layer thickness

δ^*	Displacement thickness
ε_m	Eddy viscosity factor in turbulence model, see Eq. 21
η_1, η_2, η_3	Directional cosines between the systems (x, y, z) and (ξ, η, ζ)
θ_{11}	Streamwise momentum thickness
ν	Fluid kinematic viscosity
ξ, η, ζ	Blade surface coordinate system, ξ is the nondimensional fraction of chord measured from the leading edge, η is the nondimensional radius as a fraction of tip radius, and ζ is the outward normal to the blade surface, see Figure 1
ρ	Fluid density
σ, s_1	Transformed boundary layer coordinates, see Eq. 10
τ_1, τ_2	Shear stress in the ξ and η directions, respectively
ψ, ϕ	Two-component vector potential, see Eq. 12
Ω	Constant angular velocity of the propeller

A DIFFERENTIAL PREDICTION METHOD FOR THREE-DIMENSIONAL LAMINAR AND TURBULENT BOUNDARY LAYERS OF ROTATING PROPELLER BLADES

Nancy C. Groves and Ming S. Chang

David Taylor Naval Ship Research and Development Center
Bethesda, Maryland 20084-5000

ABSTRACT

A general formulation is given for the three-dimensional boundary-layer flow on a rotating propeller blade. The basic equations are presented in a nonorthogonal coordinate system which rotates with the blade. Finite difference methods are used to develop a computer code for solving the laminar and turbulent boundary-layer equations. The Reynolds stress tensor is modeled by an algebraic eddy-viscosity formulation. In general, the equations are solved numerically using the standard Keller box method. However, regions of flow reversal across the boundary-layer are computed by the characteristic box method. A companion geometry computer code, developed to model propeller geometry characteristics, and an existing inviscid flow code for computing propeller blade pressures are combined with the boundary-layer computer code to form an efficient computation scheme. For a given potential-flow solution, a typical boundary-layer solution of 690 grid points requires 64 seconds CPU time on a CYBER 176 computer.

Computed results are presented for several blade geometries. The rotating segment solution compares well with analytical and experimental data. Predictions for a model propeller also compare favorably with experimental data and illustrate that two-dimensional theory may provide adequate predictions for applications where crossflow effects are not important. Geometry effects of warp and skew are shown to be small for the boundary-layer predictions on three model propellers.

1. INTRODUCTION

The ability to predict local flow properties on propeller blades will aid in the basic understanding of propulsor performance and cavitation. Knowledge of propeller viscous phenomena at model scale, such as laminar and turbulent separation, prior to testing, will lead to selection of test conditions appropriate to simulate prototype performance. Determination of the flow-field velocity distributions near the tip will improve the basic understanding of propeller tip vortex cavitation and provide information for defining the position of the shed vortex sheet in the inviscid propeller model.

This paper describes a general method for calculating the three-dimensional boundary layer around propeller blades. The solution is divided into three calculations (1) potential flow, (2) geometric parameters, and (3) boundary layer flow. The potential flow computer code adopted is the Brockett (1981) code for use at design conditions. The geometry and boundary layer codes are modifications of the codes developed by Cebeci, et al. (1978) for calculating three-dimensional laminar and turbulent boundary layers on ship hulls. The significant modifications to the Cebeci, et al. (1978) formulation, for propeller blade boundary-layer applications, include the addition of the Coriolis and centrifugal forces due to rotation, the use of a coordinate system appropriately describing propeller surfaces, and the specification of appropriate initial conditions.

The present boundary-layer formulation predicts both laminar and turbulent flow using the differential solution method. The earlier calculation methods of both Groves (1981), for propeller blades, and Arakawa, et al. (1983), for axial flow pump blades, compute only turbulent flow using a momentum integral solution method. There is much discussion regarding the merits of each of the solution methods. The momentum integral method requires considerably less computation time. The differential method is generally considered to give a more accurate and complete prediction of the flow characteristics. However, the major advantage of the present solution procedure is its capability of predicting laminar flow. This region is particularly important for model propeller applications where a large region of the flow over the blades is laminar. Additionally, laminar flow predictions are necessary for instability.

A similar differential calculation scheme has been developed by Itoh, et al. (1984) for predicting the three-dimensional laminar and turbulent boundary-layer flow on the rotating blades of axial flow pumps. The present calcu-

lation procedure varies from their method in two major respects. First, Itoh, et al. (1984) use an orthogonal coordinate system to represent an axial flow pump blade. While this system simplifies the governing flow equations, it encounters difficulties in grid generation for blades which deviate from a fan shape. A more general surface coordinate system defined in terms of x_C, fraction of chord measured from the leading edge, and x_R, fraction of tip radius, is chosen for the present study. The use of this coordinate system alleviates any problems associated with the calculation grid. The second variation from the work of Itoh, et al. (1984) is the specification of the initial conditions at the leading edge and the hub. Itoh, et al. (1984) applied the usual leading edge and hub conditions for three-dimensional boundaries to compute the growth for a rotating blade. Their computation diverged. In order to obtain meaningful results, they applied an averaging process to both the leading edge and the hub and developed an iterative procedure to obtain these average values within a certain accuracy. In the present study, the leading edge and hub conditions are handled differently. The methods proposed in this paper do not require an iterative procedure and the solution converges quickly for all grid points. The details of the procedures are discussed in Section 5.

The boundary-layer equations are solved numerically using the Keller (1970) two-point finite-difference method and the characteristic box procedure (see Bradshaw, et al. (1981)) for computing regions of reverse crossflow. A turbulence model is required for closure of the turbulent boundary-layer equations. The zero-order eddy-viscosity model with gradual transition, given by Cebeci and Smith (1974), is adopted here.

Even though the present analysis allows computation of the three-dimensional laminar and turbulent boundary-layer on the complex propeller blade geometry, two desirable flow predictions are beyond the scope of this study. These are the complex hub interaction and the flow transition calculation. No hub interaction is considered and the location of transition is an input parameter to the computer code determined by the user. It should be noted that the restriction of computing at design conditions only is a limitation of the Brockett (1981) formulation and not of the boundary-layer formulation. The boundary layer may be computed with any potential flow and associated blade offsets. Finally, there is no distinction in the boundary-layer solution procedure between the pressure and suction blade surfaces. The differences between the surfaces are accounted for in the potential flow and geometry calculations.

Results of the propeller blade boundary-layer calculation are presented for several geometries. The first blade studied is the large chordlength segment investigated experimentally and analytically by Lakshminarayana, et al. (1972). The laminar predictions for the blade are in agreement with the computed results of both Banks and Gadd (1962) for a rotating sector and Morris (1981) for a rotating helical blade. Overall, the turbulent predictions agree well with both the experimental data of Lakshminarayana, et al. (1972) and the analytical values of Cham and Head (1969) for the limiting case of a rotating disk. Discrepancies occur in the limiting streamline angle β which is consistently over-predicted by the present method. The second blade evaluated is a model propeller designed at DTNSRDC by Denny (1968) and tested in the DTNSRDC 12-in. water tunnel by Jessup, et al. (1984). Both two- and three-dimensional calculations were made for this blade. The results show that two-dimensional theory can adequately predict the measured data as well as three-dimensional theory with the exception of the crossflow. The final geometries investigated are an unwarped, a warped, and a skewed model propeller, examined earlier by Groves (1981), with no experimental boundary-layer data available. The current predictions show little variation in the predicted local skin friction coefficient for the three blades.

2. COORDINATE SYSTEMS

Figure 1 depicts a typical propeller blade and hub configuration. In practice, there are N symmetrically-spaced identical blades attached to the hub, but, for clarity, only one is shown in Figure 1. The propeller rotates with the constant angular velocity Ω about the x-axis. The Cartesian x, y, z, coordinate system is fixed in space and does not rotate with the blade. In this system, x is the axis of rotation, with positive displacement measured aft; z is taken as upward positive; and y forms a right-handed orthogonal system as shown in Figure 1. In the present calculation scheme, the blade geometry and potential velocities are initially specified in the Cartesian system by the Brockett (1981) lifting surface computer code.

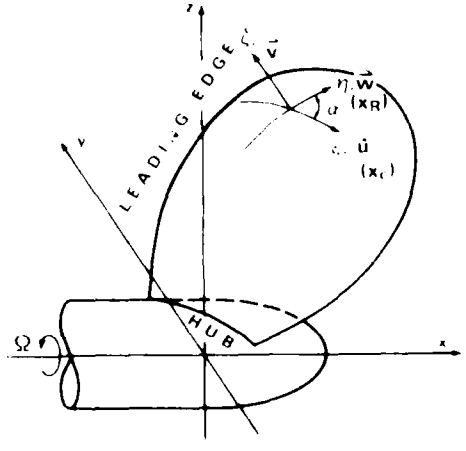

Fig. 1 - Schematic of Blade Coordinate Systems

Although the Cartesian coordinate system could be used for the boundary-layer solution procedure, a system fixed to the blade surface and rotating with the blade is chosen for its convenient representation of the complex geometry. The surface coordinates ξ, η, and ζ are defined with ξ equal to the nondimensional fraction of chord measured from the leading edge; η equal to the nondimensional radius as a fraction of the tip radius; and ζ equal to the outward normal to the blade surface. These coordinates are also illustrated in Figure 1, where α is shown as the angle between the ξ and η surface coordinates. The velocity components u, v, and w are defined in the ξ, ζ, and η directions, respectively.

The ξ and η coordinates, the Cartesian offsets on the blade reference surface (i.e., no blade thickness), and the velocity components in a helical reference frame are standard quantities produced by the Brockett lifting surface (1981) computer code. In preparation for its use in the present computation system, the Brockett code (1981) has been modified to calculate the Cartesian offsets on the actual blade surfaces and the velocities in the Cartesian reference frame. The surface offsets are needed to define certain derivative quantities i.e., the metric coefficients, geodesic curvatures, etc., used in the boundary-layer solution. Metric coefficients, denoted by h_1, h_2, and h_3 for the ξ, η, and ζ coordinates, respectively, correlate surface distances between the Cartesian and surface coordinate systems. As is typical practice in boundary-layer formulations, the boundary layer thickness is assumed to be small and the ζ coordinate is assumed to measure distance along the surface normal. Therefore, the metric h_3 is set to unity with no loss of generality. The remaining metric coefficients are defined as

$$h_1 = \left[\left(\frac{\partial x}{\partial \xi}\right)^2 + \left(\frac{\partial y}{\partial \xi}\right)^2 + \left(\frac{\partial z}{\partial \xi}\right)^2\right]^{1/2}$$

$$h_2 = \left[\left(\frac{\partial x}{\partial \eta}\right)^2 + \left(\frac{\partial y}{\partial \eta}\right)^2 + \left(\frac{\partial z}{\partial \eta}\right)^2\right]^{1/2}$$

3. BOUNDARY LAYER EQUATIONS

The steady, incompressible boundary layer equations for rotational flow in a nonorthogonal coordinate system are given by Yamazaki (1981). The equations are identical to those presented by Cebeci, et al. (1978), with the addition of two terms in the momentum equations representing the centrifugal and Coriolis forces. The governing equations, using the surface coordinates ξ, η, and ζ, are:

Continuity:

$$\frac{\partial}{\partial \xi}(uh_2\sin\alpha) + \frac{\partial}{\partial \eta}(wh_1\sin\alpha) + \frac{\partial}{\partial \zeta}(vh_1h_2\sin\alpha) = 0 \qquad (1)$$

ξ-Momentum:

$$\frac{u}{h_1}\frac{\partial u}{\partial \xi} + \frac{w}{h_2}\frac{\partial u}{\partial \eta} + v\frac{\partial u}{\partial \zeta} - K_1u^2\cot\alpha + K_2w^2\csc\alpha + K_{12}uw + 2\Omega(w+u\cos\alpha)\eta_1\csc\alpha + \Omega^2(\eta_2\eta\cot\alpha\csc\alpha) \qquad (2)$$

$$= \frac{-\csc^2\alpha}{h_1}\frac{\partial}{\partial \xi}\left(\frac{p}{\rho}\right) + \frac{\cot\alpha\csc\alpha}{h_2}\frac{\partial}{\partial \eta}\left(\frac{p}{\rho}\right) + \frac{\partial \tau_1}{\partial \zeta}$$

η-Momentum:

$$\frac{u}{h_1}\frac{\partial w}{\partial \xi} + \frac{w}{h_2}\frac{\partial w}{\partial \eta} + v\frac{\partial w}{\partial \zeta} - K_2w^2\cot\alpha + K_1u^2\csc\alpha + K_{21}uw - 2\Omega(u+w\cos\alpha)\eta_1\csc\alpha - \Omega^2\eta_2\eta\csc^2\alpha \qquad (3)$$

$$= -\frac{\csc^2\alpha}{h_2}\frac{\partial}{\partial \eta}\left(\frac{p}{\rho}\right) + \frac{\cot\alpha\csc\alpha}{h_1}\frac{\partial}{\partial \xi}\left(\frac{p}{\rho}\right) + \frac{\partial \tau_2}{\partial \zeta}$$

In these equations, u, v, and w represent the velocity components in the ξ, ζ, and η directions, respectively, α is the angle between the surface coordinates ξ and η, and Ω is the constant angular velocity. The metric coefficients h_1 and h_2 were defined in the previous section. The quantities K_1 and K_2 are the geodesic curvatures of the curves η=constant and ξ=constant, respectively, and are defined by

$$K_1 = \frac{1}{h_1h_2\sin\alpha}\left[\frac{\partial(h_2\cos\alpha)}{\partial \xi} - \frac{\partial h_1}{\partial \eta}\right] \qquad (4a)$$

$$K_2 = \frac{1}{h_1h_2\sin\alpha}\left[\frac{\partial(h_1\cos\alpha)}{\partial \eta} - \frac{\partial h_2}{\partial \xi}\right] \qquad (4b)$$

The parameters K_{12} and K_{21} are defined in terms of the geometry as

$$K_{12} = \frac{1}{\sin\alpha} - K_1 + \frac{1}{h_1}\frac{\partial \alpha}{\partial \xi} + \cos\alpha K_2 + \frac{1}{h_2}\frac{\partial \alpha}{\partial \eta} \qquad (5a)$$

$$K_{21} = \frac{1}{\sin\alpha} - K_2 + \frac{1}{h_2}\frac{\partial \alpha}{\partial \eta} + \cos\alpha K_1 + \frac{1}{h_1}\frac{\partial \alpha}{\partial \xi} \qquad (5b)$$

The remaining parameters in the boundary layer equations are:

p = static pressure in the fluid
ρ = fluid density
τ = shear stress in the ξ-direction, $\tau_1 = \nu\frac{\partial u}{\partial \zeta} - \overline{u'v'}$

τ_2 = shear stress in the η-direction, (6)

$$\tau_2 = \nu \frac{\partial u}{\partial \zeta} - \overline{v'w'}$$

ν = kinematic viscosity of the fluid

$\overline{u'v'}$, $\overline{v'w'}$ = Reynolds stresses
Ω = constant angular velocity of propeller
η_1, η_2, η_3 = directional cosines between the systems (x, y, z) and (ξ, η, ζ)

The boundary layer thickness is denoted by δ and the boundary layer is defined in the region $0<\zeta<\delta$. The boundary conditions are:

$$\zeta=0,\ u=v=w=0$$
$$\zeta=\delta,\ u=u_e(\xi,\eta),\ w=w_e(\xi,\eta) \qquad (7)$$

The pressure gradients are determined from the momentum equations at the edge of the boundary layer. The edge equations are

ξ-momentum:

$$\frac{u_e}{h_1}\frac{\partial u_e}{\partial \xi} + \frac{w_e}{h_2}\frac{\partial u_e}{\partial \eta} - K_1 u_e^2 \cot\alpha + K_2 w_e^2 \csc\alpha$$
$$+ K_{12} u_e w_e + 2\Omega(w_e + u_e\cos\alpha)\eta_1 \csc\alpha \qquad (8)$$
$$+ \Omega^2 \eta_2 \eta \cos\alpha \csc^2\alpha = -\frac{\csc^2\alpha}{h_1}\frac{\partial}{\partial \xi}\left(\frac{p_e}{\rho}\right)$$
$$+ \frac{\cot\alpha\csc\alpha}{h_2}\frac{\partial}{\partial \eta}\left(\frac{p_e}{\rho}\right)$$

η-momentum:

$$\frac{u_e}{h_1}\frac{\partial w_e}{\partial \xi} + \frac{w_e}{h_2}\frac{\partial w_e}{\partial \eta} - K_2 w_e^2 \cot\alpha + K_1 u_e^2 \csc\alpha$$
$$+ K_{21} u_e w_e - 2\Omega(u_e + w_e\cos\alpha)\eta_1 \csc\alpha \qquad (9)$$
$$- \Omega^2 \eta_2 \eta \csc^2\alpha = -\frac{\csc^2\alpha}{h_2}\frac{\partial}{\partial \eta}\left(\frac{p_e}{\rho}\right) + \frac{\cot\alpha\csc\alpha}{h_1}\frac{\partial}{\partial \xi}\left(\frac{p_e}{\rho}\right)$$

Transformed variables are defined as

$$\xi = \xi,\quad \eta = \eta,\quad d\sigma = \frac{u_e^{1/2}}{\nu s_1}\,d\zeta,\quad s_1 = \int_0^{\xi} h_1 d\xi \qquad (10)$$

A two component vector potential is introduced with

$$u h_2 \sin\alpha = \frac{\partial \psi}{\partial \zeta} \qquad (11)$$
$$w h_1 \sin\alpha = \frac{\partial \phi}{\partial \zeta}$$
$$v h_1 h_2 \sin\alpha = -\left(\frac{\partial \psi}{\partial \xi} + \frac{\partial \phi}{\partial \eta}\right)$$

where ψ and ϕ are defined as

$$\psi = (\nu s_1 u_e)^{1/2} h_2 \sin\alpha\, f(\xi,\eta,\sigma) \qquad (12)$$
$$\phi = (\nu s_1 u_e)^{1/2} \frac{u_{ref}}{u_e} h_1 \sin\alpha\, g(\xi,\eta,\sigma)$$

and u_{ref} is a reference velocity.

The potential velocities u, v, and w are rewritten using the vector potentials ψ and ϕ, the Reynolds stresses are rewritten in terms of the eddy viscosity factor ε_m, and the boundary-layer edge conditions are applied to eliminate the pressure terms. The transformed ξ- and η-equations are

ξ-momentum: $(bf'')' + m_1 ff'' - m_2(f')^2 - m_5 f'g'$
$+ m_6 f''g - m_8(g')^2 + m_{11} - m_{13}f' - m_{14}g' + m_{15}$
$= m_{10}\left(f'\frac{\partial f'}{\partial \xi} - f''\frac{\partial f}{\partial \xi}\right) + m_7\left(g'\frac{\partial f'}{\partial \eta} - f''\frac{\partial g}{\partial \eta}\right) \qquad (13)$

η-momentum:

$(bg'')' + m_1 fg'' - m_4 f'g' - m_3(g')^2 + m_6 gg''$
$- m_9(f')^2 + m_{12} + m_{16}f' + m_{13}g' - m_{17}$
$= m_{10}\left(f'\frac{\partial g'}{\partial \xi} - g''\frac{\partial f}{\partial \xi}\right) + m_7\left(g'\frac{\partial g'}{\partial \eta} - g''\frac{\partial g}{\partial \eta}\right) \qquad (14)$

In these equations, primes denote differentiation with respect to σ and

$$f' = \frac{u}{u_e},\quad g' = \frac{w}{u_{ref}},\quad b = 1 + \frac{\varepsilon_m}{\nu} \qquad (15)$$

The coefficient terms m_1 through m_{12}, identical to those given by Cebeci, et al. (1978), are

$$m_1 = \frac{1}{2}\left(1 + \frac{s_1}{h_1 u_e}\frac{\partial u_e}{\partial \xi}\right) + \frac{s_1}{h_1 h_2 \sin\alpha}\frac{\partial}{\partial \xi}(h_2 \sin\alpha)$$
$$m_2 = \frac{s_1}{h_1 u_e}\frac{\partial u_e}{\partial \xi} - s_1 K_1 \cot\alpha$$
$$m_3 = -s_1 K_2 \frac{u_{ref}}{u_e}\cot\alpha$$
$$m_4 = s_1 K_{21}$$
$$m_5 = \frac{s_1}{h_2}\frac{u_{ref}}{u_e^2}\frac{\partial u_e}{\partial \eta} + s_1 K_{12}\frac{u_{ref}}{u_e}$$
$$m_6 = \frac{s_1}{h_1 h_2 \sin\alpha}\frac{1}{\bar{u}_e \bar{s}_1}\frac{\partial}{\partial \eta}\left(\bar{u}_e \bar{s}_1 h_1 \sin\alpha\frac{u_{ref}}{u_e}\right) \qquad (16)$$
$$m_7 = \frac{s_1}{h_2}\frac{u_{ref}}{u_e}$$
$$m_8 = s_1 K_2 \frac{u_{ref}^2}{u_e}\csc\alpha$$

Copies	
2	McDonnell Douglas, Long Beach 1 T. Cebeci 1 J.L. Hess
1	Newport News Shipbuilding/Lib
1	Nielsen Eng & Research
1	Rand Corp
1	Rockwell International 1 B. Ujihara
1	Sperry Rand/Tech Lib
1	Stanford Research Inst/Lib
1	TRW Systems Group/Lib
1	United Technology/East Hartford, Conn
2	Westinghouse Electric 1 M.S. Macovsky 1 Gulino
1	Woods Hole Oceanographic, Inc./ Ocean Eng Dept

CENTER DISTRIBUTION

Copies	Code	Name
1	1500	W.B. Morgan
1	1504	A.J. Monacella
1	1506	S. Hawkins
1	1508	R. Boswell
1	152	W.C. Lin
1	1522	C.H. Sung
1	154	J. McCarthy
1	1542	T.T. Huang
5	1542	N.C. Groves
1	1542	Y.T. Lee
1	1542	M.S. Chang
1	1544	F. Peterson
1	1544	S. Jessup

CENTER DISTRIBUTION (Continued)

Copies	Code	Name
1	156	D.S. Cieslowski
1	1606	T.C. Tai
1	1802.1	H. Lugt
1	1840	J. Schot
1	19	M.M. Sevik
10	5211.1	Reports Distribution
1	522.1	TIC (C)
1	522.2	TIC (A)

Copies	
1	Cornell U/Shen
2	Harvard U 1 G. Carrier 1 Gordon McKay Lib
1	U of Illinois/J. Robertson
4	U of Iowa 1 Lib 1 L. Landweber 1 V.C. Patel 1 C.J. Shen
1	Johns Hopkins U/Lib
4	MIT 1 Lib 1 J.R. Kerwin 1 T.F. Ogilvie 1 J.N. Newman
1	U of Minn/St. Anthony Falls 1 R. Arndt
1	U of Mich/NAME/Lib
1	U of Notre Dame/Eng Lib
1	New York U/Courant Inst/Lib
1	Penn State/ARL Lib
1	Princeton U/Mellor
1	U of Rhode Island/F.M. White
1	Science Application, Inc. Annapolis, MD C. von Kerczek
1	SIT/Lib
1	U of Texas/Arl Lib
1	Utah State U/Jeppson
1	Southwest Res Inst 1 Applied Mech Rev

Copies	
2	Stanford U 1 R. Street, Dept Civil Eng 1 S.J. Kline, Dept Mech Eng
1	Stanford Res Inst/Lib
1	U of Virginia Inst/Lib
1	U of Virginia/Aero Eng Dept
1	U of Washington/Arl Tech Lib
1	U.S. Naval Academy
1	VPI 1 J. Schetz, Dept Aero & Ocean Eng
2	Webb Inst 1 Lib 1 Ward
1	Worchester PI/Tech Lib
1	SNAME/Tech Lib
1	Bell Aerospace
1	National Science Foundation/ Eng Div Lib
1	Boeing Company/Seattle/Marine System
1	Bolt, Beranek & Newman/Lib
1	General Dynamics, EB/Boatwright
1	Flow Research
1	Gibbs & Cox/Tech Info
1	Grumman Aerospace Corp 1 Lib
1	Hydronautics/Lib
1	Lockheed, Sunnyvale/Waid

INITIAL DISTRIBUTION

Copies	
1	WES
1	U.S. ARMY TRAS R&D Marine Trans Div
3	ONR/432F Whitehead, Lee, Reischman
2	NRL 1 Code 2027 1 Code 2629
1	NORDA
2	USNA 1 Tech Lib 1 B. Johnson
2	NAVPGSCOL 1 T. Sarpkaya 1 J. Miller
1	NOSC/Lib
1	NCSC/712
1	NCEL/131
1	NSWC, White Oak/Lib
1	NSWC, Dahlgren/Lib
1	NUSC/Lib
11	NAVSEA 1 SEA 99612 (Library) 1 SEA 05R24 (J. Sejd) 1 SEA 55W3 (E. Comstock) 1 SEA 55W33 (W. Sandburg) 1 SEA 55W31 (W. Louis) 1 SEA 55W31 (G. Jones) 1 SEA 55N2 (A. Paladino) 1 SEA 55N1 (S.G. Wieczorek) 1 SEA 63R31 (T. Peirce) 1 SEA 56X12 (C.R. Crockett) 1 SEA 62R41 (L. Pasiuk)
1	NAVFAC/032C

Copies	
1	NADC
1	NAVSEC, NORVA/6660.03, Blount
12	DTIC
1	AFOSR/NAM
1	AFFOL/FYS, J. Olsen
1	MARAD 1 Div of Ship R&D
1	NASA/HQ/Lib
2	NASA/Ames Res Ctr, Lib 1 D. Kwak 1 J.L. Steger
1	NASA/Langley Res Ctr 1 D. Bushnell
1	NBS/Lib
1	LC/Sci & Tech
1	DOT/Lib TAD-491.1
1	MMA 1 Lib
2	U of Cal/Dept Naval Arch, Berkeley 1 W. Webster 1 R. Yeung
2	U of Cal., San Diego 1 A.T. Ellis 1 Scripps Inst Lib
1	U of Cal., Santa Barbara/Tulin
2	CIT 1 Aero Lib 1 A.J. Acosta
1	Colorado State U/Eng Res Ctr

ACKNOWLEDGEMENTS

This work was funded under the DTNSRDC General Hydrodynamics Research Program, Work Unit 1542-103, Task Area ZR0230101, Program Element 61152N.

The authors would like to thank Dr. Thomas T. Huang for his continuous support and technical guidance. Special appreciation is extended to Dr. Yu-Tai Lee and to Dr. Tuncer Cebeci of the University of California, Long Beach for their technical discussion in the difference scheme used in this paper. The authors also wish to acknowledge Ms. Lauri Jeantheau for her patient and accurate typing of the paper.

REFERENCES

Arakawa, C., T. Tagori, and M. Shirakura (1983): Analysis of Three-Dimensional Turbulent Boundary Layer on the Rotating Blade of Axial Flow Pump. Trans. JSME, 49-437(B).

Banks, W.H.H. and G.E. Gadd (1962): A Preliminary Report on Boundary Layers on Screw Propellers and Simpler Rotating Bodies. Nat. Physics Lab. Report SHR27.

Bradshaw, P., T. Cebeci and J.H. Whitelaw (1981): **Engineering Calculation Methods for Turbulent Flow.** Academic Press, New York.

Bradshaw, P., D.H. Ferriss, and N.P. Atwell (1967): Calculation of Boundary-Layer Development Using the Turbulent Energy Equation. **J. Fluid Mech.**, Vol. 28.

Brockett, T. (1981): Lifting Surface Hydrodynamics for Design of Rotating Blades. **PROPELLERS '81,** Virginia Beach, Va; Published by The Society of Naval Architects and Marine Engineers, New York.

Cebeci, T. and P. Bradshaw (1977). **Momentum Transfer in Boundary Layers.** Hemisphere-McGraw Hill, Washington.

Cebeci, T. and A.M.O. Smith (1974): Analysis of Turbulent Boundary Layers. **Applied Mathematics Mechanics,** Vol. 15, Academic Press, New York.

Cebeci, T., K.C. Chang, and K. Kaups (1978): A General Method for Calculating Three-Dimensional Laminar and Turbulent Boundary Layers on Ship Hulls. MDC J7998.

Cebeci, T., K. Kaups, and J.A. Ramsey (1977): A General Method for Calculating Three-Dimensional Compressible Laminar and Turbulent Boundary Layers on Arbitrary Wings. NASA CR-2777.

Cham, T.S. and M.R. Head (1969): The Turbulent Boundary-Layer Flow on a Rotating Disk. **J. Fluid Mech.**, Vol. 37, part 1, pp. 129-147.

Denny, S.B. (1968): Cavitation and Open-Water Performance Tests of a Series of Propellers Designed by Lifting Surface Methods. DTNSRDC Report 2878.

Groves, N.C. (1981): An Integral Prediction Method for Three-Dimensional Turbulent Boundary Layers on Rotating Blades. **PROPELLERS '81,** Virginia Beach, Va; Published by The Society of Naval Architects and Marine Engineers, New York.

Itoh, S., C. Arakawa, and T. Tagori (1984): Differential Method of 3-D Boundary Layer on the Rotating Blade of Axial Flow Pump. **Journal of Japan,** Vol. 50, No. 454B; Published by Association for Mechanical Engineers.

Jessup, S.D., C. Shott, M. Jeffers, and S. Kobayashi (1984): Local Propeller Blade Flows in Uniform and Sheared Onset Streams Using LDV Techniques. **Fifteenth ONR Symposium on Naval Hydrodynamics,** Hamburg.

Keller, H.B. (1970): A New Difference Scheme for Parabolic Problems. **Numerical Solution of Partial-Differential Equations,** J. Bramble (ed.), Vol. 2, Academic Press, New York.

Lakshminarayana, B., A. Jabbari, and H. Yamaoka (1972): Turbulent Boundary Layer on Rotating Helical Blade. **J. Fluid Mech.,** Vol. 51, Part 3, pp. 545-569.

Morris, P.J. (1981): The Three-Dimensional Boundary Layer on a Rotating Helical Blade. **J. Fluid Mech.,** Vol. 112, pp. 283-296.

Yamazaki, R. (1981): On the Theory of Marine Propellers in Non-Uniform Flow. Reprinted from the Memoirs of the Faculty of Engineering, Kyushu University, Vol. 41, No. 3.

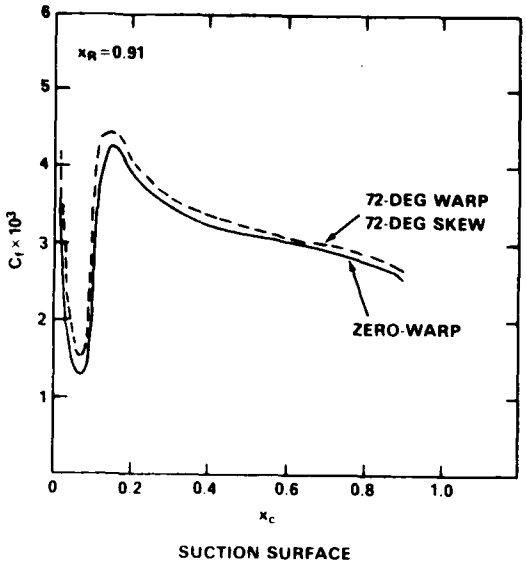

Fig. 16 - Variation of Streamwise Skin Friction Coefficient on Three Model Propellers

chord value x_C = 0.18. The design advance coefficient J_V of all three models is 0.889 and the flow conditions are $\nu = 1.191 \times 10^{-6}$ m^2/s (1.28×10^{-5} ft^2/sec), V=16.9 m/s (55.3 ft/sec), and Ω = 391.5 rad/sec.

Figure 16 shows the predicted skin friction coefficient on the suction surface for the three model propellers at the fraction of radius value x_R = 0.91. This location corresponds to streamline 14 used for comparisons in the earlier work of Groves (1981) where the turbulent boundary layer is computed using momentum integral methods. The present results predict only a slight increase in the skin friction coefficient for the warped and skewed blades. This contradicts the results obtained by the integral method of Groves (1981) where the skin friction coefficient was predicted to increase by nearly 30 percent for the zero warp blade. An investigation into the momentum integral coding has identified an error in the specification of certain geometry parameters for these blades and thus leads to the different and erroneous earlier conclusion of Groves.

8. CONCLUSIONS

This paper presents analysis and results for computing three-dimensional laminar and turbulent boundary layers on the surface of a propeller blade using the differential method. The solution procedure is a modification of the Cebeci, et al. (1978) scheme for boundary-layer calculations on three-dimensional ship hulls. The major changes to the scheme result from the propeller blade rotation, the complex propeller geometry, and the specification of initial conditions in order to begin the calculation procedure. Typical boundary layer computations use a grid of 30 chordwise and 23 radial points thereby covering the entire blade surface. For this grid size, 64 seconds CPU time on a CYBER 176 computer are required for a complete calculation.

Overall, the predicted boundary-layer parameters are shown to give reasonable agreement with experimental data for both simple (rotating disk and rotating helical segment) bodies and a model propeller. The largest discrepancies between the current predictions and experimental data and previous theories occur for the limiting streamline angle β which is overpredicted in the turbulent region. For the rotating segment, this parameter is shown to be correctly computed by the differential method in the laminar region. For turbulent flows, momentum integral methods, which include a modified entrainment function to account for rotational effects, have been shown (see Banks and Gadd (1962) and Groves (1981)) to improve the prediction of tanβ. The viscosity coefficient in the present differential method has not been modified. The value of tanβ may be reduced if the eddy viscosity were modeled more precisely.

The analysis of model Propeller 4119 has provided insight into the boundary-layer calculation on propeller blades. First, the large extent of laminar flow on the model blade necessitates the capability of a laminar calculation procedure and an instability prediction method to determine the transition location. Figures 9 through 13 show that two-dimensional theory can be used for the prediction of boundary-layer parameters such as chordwise velocity profiles, shape factor, and chordwise skin friction. However, applications involving crossflow, such as the instability calculation or tip vortex investigations, require the full three-dimensional computation. Figures 9 and 14 show the dangers of using a partially rotating three-dimensional calculation. Incorrect values of the crossflow velocities and tanβ are predicted when rotation is included in the potential-flow solution and not included in the boundary-layer solution.

Calculations of the three-dimensional boundary-layer characteristics of three model propellers of varying geometry indicate only slight differences in the skin friction parameters; see Figure 16. This result, contrary to the earlier momentum integral result of Groves (1981), led to the discovery of a geometry error in the earlier computer code.

The results in this paper are encouraging. Although computed with the present preliminary version of the code, comparisons with measured data are quite good. Further code modifications are anticipated to allow the calculation to proceed past the location of turbulent separation and to improve the eddy viscosity model. Additional comparisons will be made with the experimental data of Itoh, et al. (1984) for a rotating axial flow pump blade.

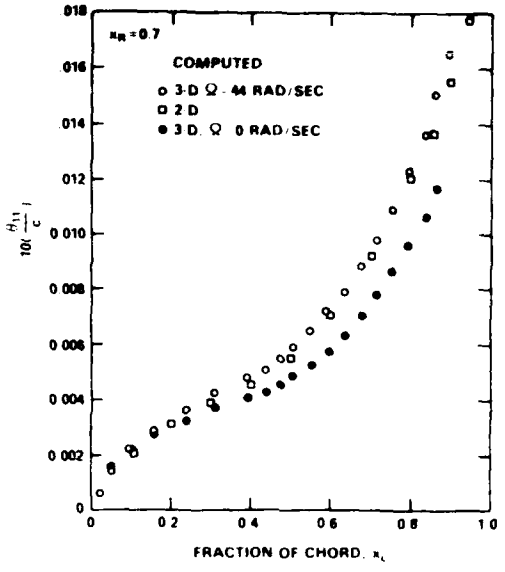

Fig. 13 - Variation of Streamwise Momentum Thickness on Model 4119

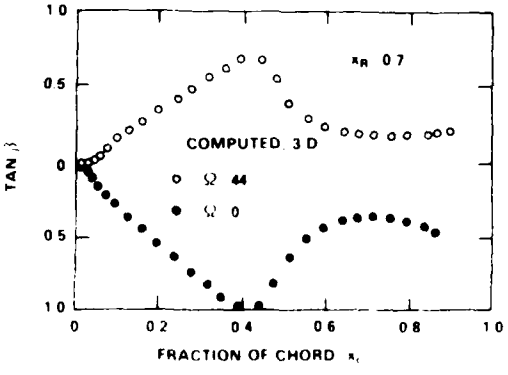

Fig. 14 - Variation of Limiting Streamline Angle on Model 4119

meter is positive for flow with rotation and negative for flow with no rotation, as predicted for the radial velocity distribution.

To summarize, the boundary layer characteristics of a propeller blade can be computed with reasonable accuracy. Two dimensional theory gives excellent predictions of the flow for applications where crossflow is not important. Applications where the crossflow is important, including model propeller studies where large regions of laminar flow exist and in the study of instability, require use of the full three-dimensional equations. The use of three-dimensional theory without including rotation in the boundary-layer solution should be avoided.

7.3 Skewed and Warped Propellers

In this section, results are presented for the computed boundary-layer characteristics of three analytically-defined propeller blades. These three 0.30 m (1 ft) diameter model propellers were chosen to investigate the effects of varying geometry on boundary-layer flow. The propellers, denoted as Model 4381, an unwarped blade; Model 4498, a 72-degree warped blade; and Model 4383, a 72-degree skewed blade, are depicted in Figure 15. The complete geometry of these model propellers is given in Groves (1981) and is not repeated here.

Since no experimental data exist for these particular models, the transition location must be estimated. Unpublished experimental results at DTNSRDC on a similar geometry indicate that the flow over the blades is fully turbulent at a 0.7-radius Reynolds number of 4×10^6. This Reynolds number corresponds to tripping the boundary layer at the fraction of

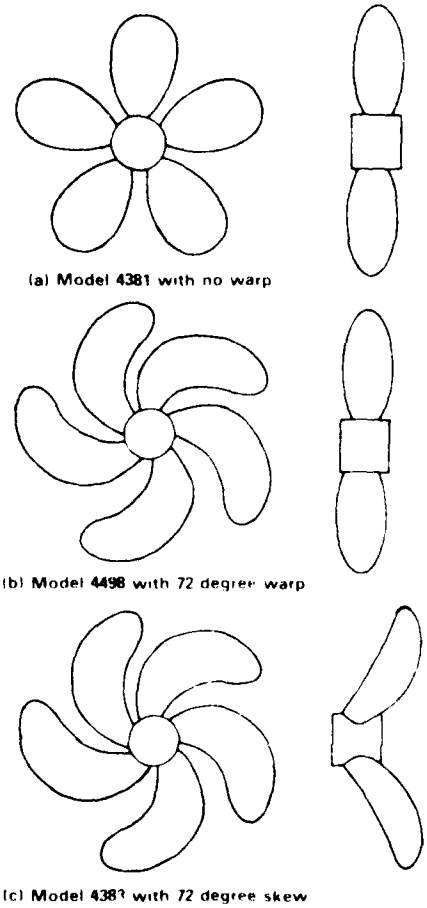

(a) Model 4381 with no warp

(b) Model 4498 with 72 degree warp

(c) Model 4383 with 72 degree skew

Fig. 15 - Geometry of Three Model Propellers

and the chordwise velocity u. In addition, the momentum thickness θ_{11} and skin friction coefficient C_f are compared with two-dimensional predictions from a computer code developed by Cebeci (1978). The radial velocity w and the limiting streamline angle β are the two parameters shown which are unique to three-dimensional flow. No measurement has been made of these quantities as yet. A second calculation was made using the present method. This calculation is performed with the rotational effects included in the potential-flow velocities but not in the boundary-layer computation. These results, which approximate the rotating flow above a solid ground, are also presented.

Figures 9 through 14 show the boundary-layer comparisons for Model 4119. The series of dashed and dotted lines in Figures 9a through 9c represent Jessup's (1984) measured chordwise velocity profiles for the three blades at three chordwise locations, x_c = 0.1, 0.4, 0.8, respectively. The boundary layer is shown to thicken considerably as the blade trailing edge is approached. The open circles and squares, denoting the fully-rotational three-dimensional calculation and the two-dimensional calculation, respectively, are both shown to approximate the measured chordwise profiles equally as well. However, the calculation without the rotation in the boundary layer overpredicts the velocity. It is further seen from Figure 9 that disregarding the rotational effects in the boundary-layer computation leads to the prediction of an inward rather than an outward radial flow. An inward flow contradicts the flow visualization results of Jessup (1984).

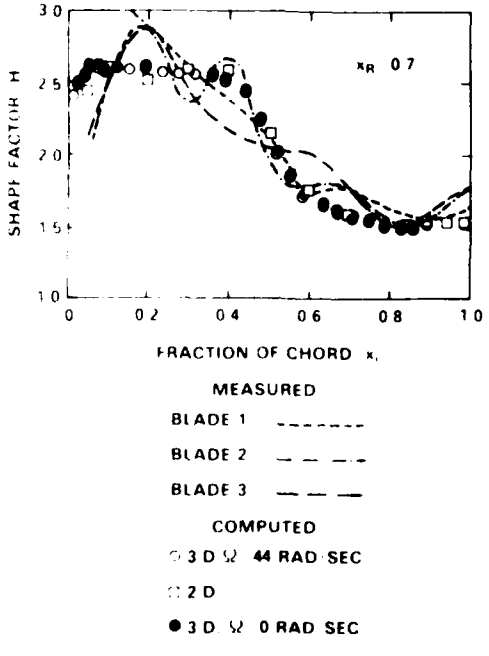

Fig. 10 - Variation of Shape Factor on Model 4119

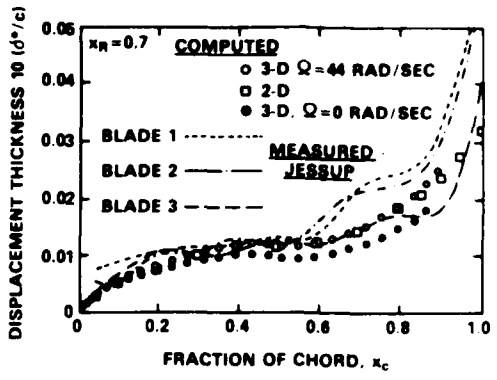

Fig. 11 - Variation of Displacement Thickness on Model 4119

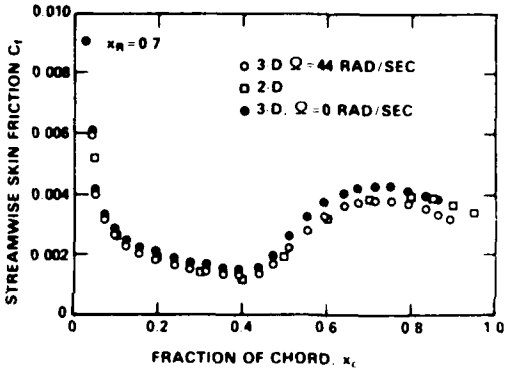

Fig. 12 - Variation of Streamwise Skin Friction Coefficient on Model 4119

Considerable scatter is noted in Figure 10 for the measured shape factor parameter H. Nevertheless, the overall character of the variable is reasonably well-predicted by the various theoretical methods, including the three-dimensional boundary layer without rotation. The displacement thickness, shown in Figure 11 is again well-predicted by two-dimensional flow theory and three-dimensional flow theory with rotation. Without the rotational effects, three-dimensional flow is shown to underpredict the displacement thickness.

Jessup (1984) does not present measurements for either the streamwise skin friction coefficient C_f or the momentum thickness θ_{11}. Comparisons of the calculated values of C_f and θ_{11} are given in Figures 12 and 13. Again, two-dimensional theory agrees well with three-dimensional predictions with rotation and both disagree somewhat with three-dimensional predictions with no rotation.

Finally, the tangent of the limiting streamline angle β is compared in Figure 14 for the three-dimensional calculations with and without rotation. Unsurprisingly, this para-

8, taken from Cham and Head (1969), shows comparisons of experimental data with several calculation methods. The circled asterisks denoting the present predictions are in good agreement with both previous theories and measured data.

In summary, the present differential method solution procedure has been shown to accurately predict both laminar and turbulent boundary-layer characteristics on a simple three-dimensional blade. The previous momentum integral methods of Groves (1981) and Arakawa, et al. (1983) could not predict laminar flow, a region important in model propeller and instability applications. The limiting streamline angle for turbulent flow is overpredicted, perhaps indicating that a change in the eddy viscosity model is needed to account for the rotation.

7.2 Propeller 4119

DTNSRDC Model Propeller 4119 (see Denny (1968) for the complete model geometry) was evaluated experimentally on the suction surface by Jessup, et al. (1984) in the DTNSRDC 24-in water tunnel. The three-bladed unskewed, propeller model has a 0.30 m (1 ft) diameter with a hub radius of 0.03 m (0.1 ft). The design advance coefficient J_V of the model is 0.833 where $J_V = V/(nD)$ and V equals the onset speed, n is the constant rotational speed in revolutions per unit time, and D is the rotor diameter. The flow conditions set for Jessup's (1984) experiments are the kinematic viscosity of 68° fresh water $\nu = 1.00 \times 10^{-6} m^2/s$ (1.08×10^{-5} ft^2/sec), the onset velocity $V = 1.83$ m/s (6.0 ft/sec) and the rotational speed $\Omega = 44$ rad/s (7 rev/sec). These conditions yield a 0.7-radius Reynolds number of $R_n = 7.3 \times 10^5$ where

$$R_n = \frac{(c)_{0.7}\, V \sqrt{1 + \left(\frac{0.7\pi}{J_V}\right)^2}}{\nu} \qquad (27)$$

and $(c)_{0.7} = 0.14$ m (0.46 ft) is the blade chord at 0.7 radius.

The 0.7 radius was chosen for comparison with Jessup's (1984) experiments since the measured data are most complete at this radius. Flow visualization techniques predict fully turbulent flow begins in the region between fraction of chord values x_c of 0.5 to 0.6. The present theoretical eddy viscosity model incorporates an intermittancy region of gradual transition from laminar to turbulent flow. The use of an intermittancy region requires an early specification of the transition location to the computational scheme. It has been determined by trial and error that an input transition location to the computational procedure of $x_c = 0.43$ yields fully turbulent flow at the chord values x_c of 0.5 to 0.6.

The boundary-layer characteristics compared with experimental data are the streamwise displacement thickness

$$\delta^* = \int_0^\infty \left(1 - \frac{u}{u_e}\right) d\zeta,$$ the shape factor $H = \delta^*/\theta$,

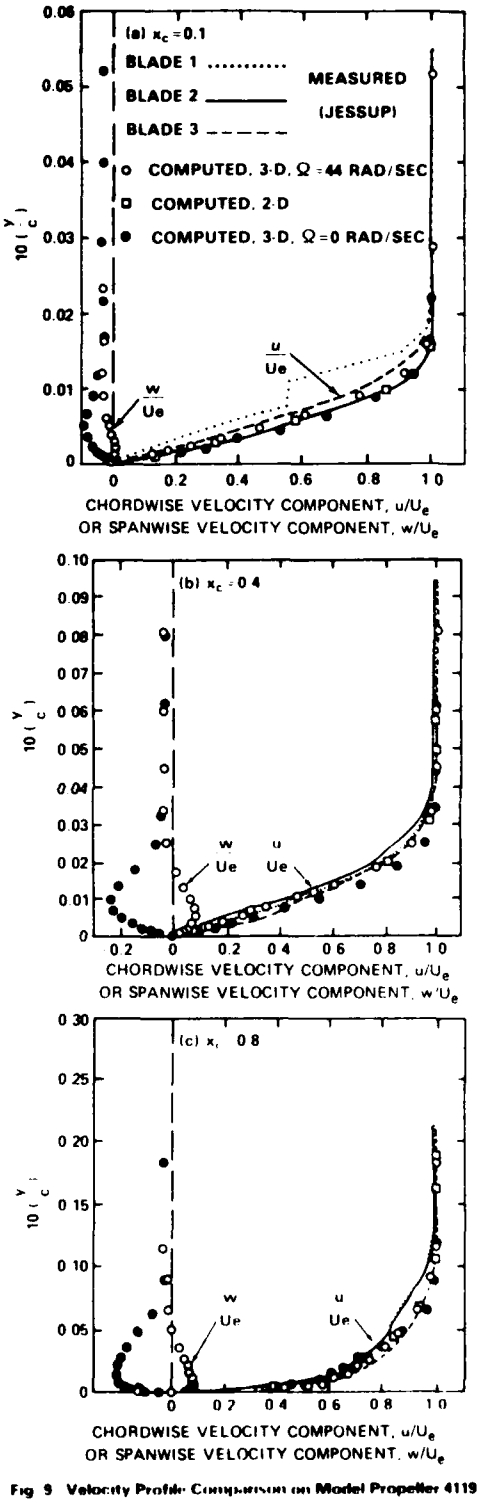

Fig 9 Velocity Profile Comparison on Model Propeller 4119

the flow parameters calculated by Lakshminarayana, et al. (1972).

Figures 5a and 5b show the momentum thickness as a function of chordwise position for fraction of radius, x_R, values of 0.72 and 0.93, respectively. The streamwise momentum thickness is defined as

$$\theta_{11} = \int_0^{\delta} \left(1 - \frac{u}{ue}\right) \frac{u}{ue} \, d\zeta$$

The dotted lines denoting the present calculation and the dashed lines denoting the calculation of Lakshminarayana, et al. are in close agreement. The experimental data are denoted by the circular symbols. At the radial location r/R = 0.72 shown in Figure 5a, all calculation methods overpredict the measured values of θ_{11} for 2 radians $< \theta <$ 5 radians. However, agreement between experiment and theory is quite good for the early stages of turbulence, $\theta <$ 2 radians, and for the blade trailing edge, $\theta \rightarrow$ 5 radians. The experimental data shown in Figure 5b at the radius r/R = 0.93 are more scattered. Agreement between experiment and theory at this radius is reasonable only for $\theta <$ 2 radians.

The tangent of the limiting streamline angle β, $\beta = \tan^{-1}\left(\frac{C_{fr}}{C_{f\theta}}\right)$, is shown in Figure 6.

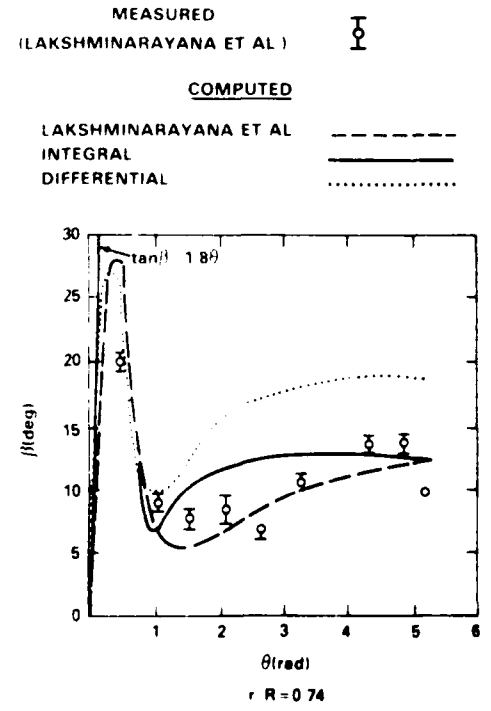

Fig. 6 - Variation of Limiting Streamline Angle β on Rotating Helical Segment

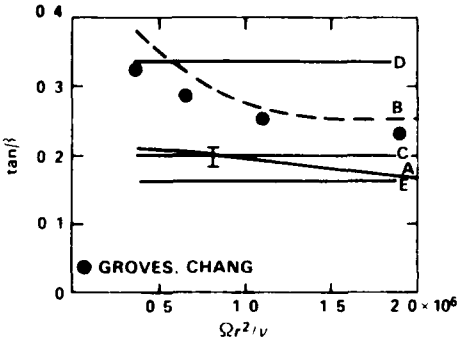

Fig. 7 - Angles of Surface Streamlines on a Rotating Disk; I , experiment; A, Cham and Head calculation using the entrainment method; B, calculation with isotropic eddy viscosity; C, Banks & Gadd (1962); D, Goldstein (1935); E, von Kármán (1921).

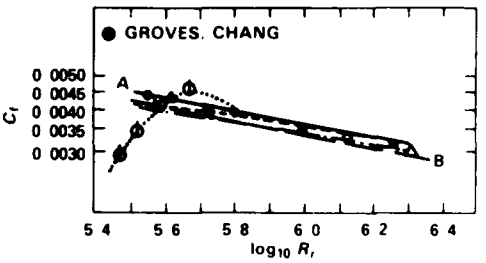

Fig. 8 - Development of the Streamwise Skin-Friction Component. —— A, Cham and Head calculation using the entrainment method; —— B, von Kármán (1921); — — , Goldstein (1935); ·····, calculation, with isotropic eddy viscosity; ·-·-· I ·-·-·, Theodorsen & Regier (1944). Results taken from Clauser plots of the present measurements: × ,515 rev/min; ○ , 1000 rev/min; △ , 1550 rev/min.

The momentum integral methods of both Lakshminarayana, et al. (1972) and Groves (1981) show closer agreement to the measured values of tanβ than does the present method. Figure 7, from the Cham and Head (1969) study of the turbulent boundary-layer flow on a disk, shows the discrepancy in various calculation methods of the parameter tanβ. As shown by the dotted line labeled B and the circular symbols denoting the present calculation method, the eddy viscosity model predicts a larger value of the limiting streamline than do the other turbulence models. Referring to Figure 6 again, the solid line labeled $\tan\beta = 1.8\theta$ shows the exact analysis result of Banks and Gadd (1962) for laminar flow on a rotating segment. The present calculation agrees well with this line. One further factor to note is that the momentum integral method of Groves (1981) included a modification to reduce the entrainment function from the flat plate value to include the rotational effect. The viscosity coefficient in the differential method has not been modified. The current tanβ prediction may be reduced if a more precise eddy viscosity model were used.

The final comparison shows the skin friction coefficient for a rotating disk. Figure

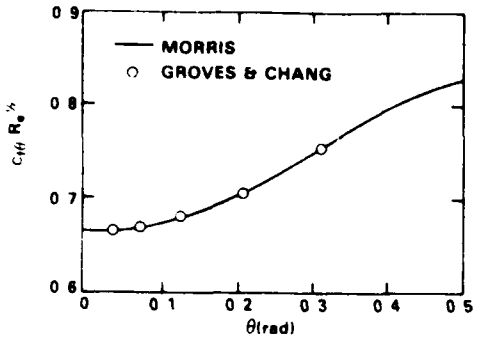

(a) STREAMWISE SKIN FRICTION COEFFICIENT

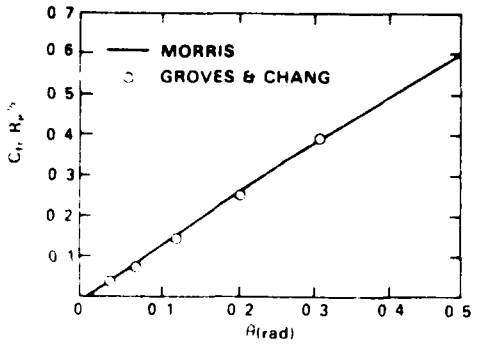

(b) RADIAL SKIN FRICTION COEFFICIENT

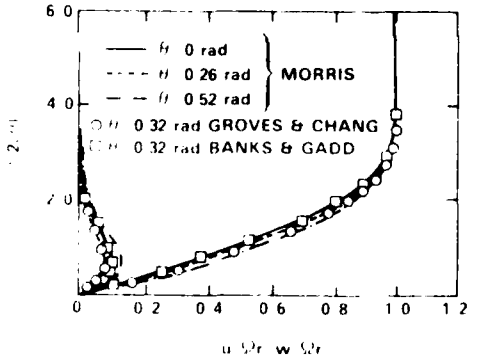

(c) VELOCITY PROFILES

Fig 4 Laminar Flow Comparisons for Rotating Helical Segment at r/R 0 95

Crosswise and radial velocity profiles are compared in Figure 4c. Morris's profiles are shown at chordwise locations of 0, 0.26, and 0.52 radians. The present predictions are shown at θ = 0.32 radians as the circle. The square symbols denote the radial and crosswise velocity of Banks and Gadd (1962) at θ = 0.32 radians. This figure shows that the laminar crosswise velocity profile is predicted quite well and the radial velocity profile is just slightly underpredicted by the present method.

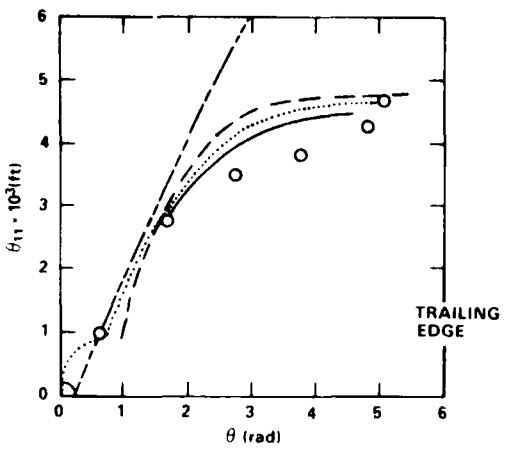

(a) r/R 0 72

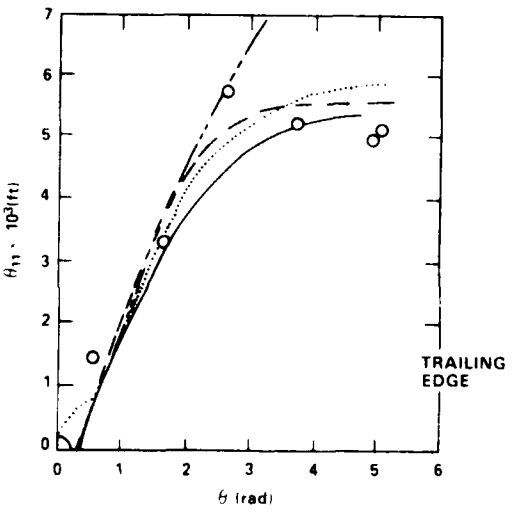

(b) r/R = 0 93

MEASURED (LAKSHMINARAYANA ET AL.)

COMPUTED
- FLAT PLATE
- LAKSHMINARAYANA ET AL
- INTEGRAL
- DIFFERENTIAL

Fig. 5 - Variation of Momentum Thickness θ_{11} on Rotating Helical Blade

A second calculation was made with transition set to θ = 0.32 radians. This location is forward of the experimentally determined transition location of θ = 0.73 radians. However, with the gradual transition model used in the current computer code, this forward transition location gives good agreement with

visualization techniques, or by assuming transition empirically. One empirical formulation which may be used is the flat-plate critical Reynolds number, $R_x = \Omega r^2\theta/\nu = 3 \times 10^5$. The input transition location is overridden if laminar separation, identified as a negative streamwise skin friction coefficient, occurs. Once transition occurs, each succeeding node is computed as turbulent. Presently, the calculations stop once turbulent separation is encountered.

7. COMPUTATIONAL RESULTS AND DISCUSSION

A variety of geometries were considered during the verification stage of the three-dimensional boundary-layer computation scheme. These geometries include a flat plate, a rotating disk, rotation above the ground, a skewed and an unskewed rotating segment, an upwarped model propeller, and three model propellers, one with warp, one with skew, and one with neither warp nor skew. Overall agreement with exact solutions and test results is quite good. The largest discrepancy with experimental data occurs for the limiting streamline angle β in turbulent flows.

Computational results are presented for the following geometries. A single, nonlifting blade of large chordlength is examined initially. Predictions in the initial laminar flow region are compared with the results of Banks and Gadd (1962) on a rotating sector and with Morris's (1981) predictions on a helical blade. The boundary layer on this blade is computed a second time with a small laminar flow region to simulate the test conditions of Lakshminarayana, et al. (1972). At large chord length, this blade approximates a rotating disk and comparisons are shown with turbulent flow solutions for a disk. To investigate the laminar flow region more extensively, the flow about a three-bladed model propeller is examined. Transition for this blade is set at 43 percent of the chord length to simulate the test data of Jessup, et al. (1984). Comparisons are made with the suction surface measurements of Jessup, et al. at the fraction of radius $x_R = 0.7$. Finally, the effects on the boundary layer of the geometry parameters warp and skew are examined using three model propellers. No experimental results exist for these blades.

7.1 Rotating Segment

The large chord length rotating segment examined is the blade generated for investigation of turbulent flow by Lakshminarayana, et al. (1972). The blade, shown in Figure 3, is a single nonlifting rotating sector of 92.6 cm (36.6 in.) diameter with a 300 degree included angle. The hub radius is 22.86 cm (0.75 ft.). The pitch/diameter ratio of 0.273 for this blade is small enough to approximate the blade by a flat circular disk with a leading and trailing edge 300 degrees apart. Present calculations are performed using the surface coordinates θ (or x_C, fraction of chord), r (or x_R, fraction of

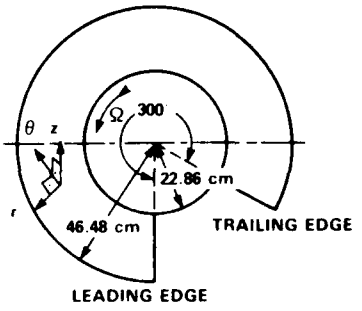

Fig. 3 - Geometry and Coordinates of Rotating Helical Segment

radius), and ζ (surface normal). For comparisons with measured data, the cylindrical coordinates (r, θ, and z) are used where r is the dimensional radius varying in the radial direction, $\theta = 300\pi/180$ radians varying in the chordwise direction, and z varies along the surface normal as $z = \zeta$.

Lakshminarayana, et al. (1972) tested the blade in a housing with a 0.20 cm (0.08in.) clearance between the blade tip and the wall. The free-stream onset flow was zero and the rotational speed of the blade, denoted Ω, remained constant at 47 rad/sec (450 rev/min). The kinematic viscosity ν equaled 1.49×10^{-5} m^2/s ($160 \times 10^{-6} ft^2/sec$) which corresponds to air at 20°C (68°F). These conditions, which yield a Reynolds number based on tip radius and tip rotational speed of 7×10^5, are used in the evaluation of the present method. In addition, present calculations begin at the blade surface location $\theta = 0.016$ radians and $x_R = r/R = 0.492$.

Initially, a boundary-layer calculation of the rotating blade was made with transition set to 1.0 radian to allow a comparison with the laminar flow predictions of Banks and Gadd (1962) on a flat sector and of Morris (1981) on a helical blade. The comparisons with the predictions of Morris (1981) are valid at large radii; the twisted blade used by Morris has not yet been evaluated with the present method. Nonetheless, the large radii comparison is important for validating the radial skin friction coefficient. Figures 4 a through c show comparisons with Morris's (1981) calculations at $r/R = 0.95$. Figures 4a and 4b compare the streamwise and radial skin friction coefficients

$$C_{f\theta} = \frac{\tau_c}{\frac{1}{2}\rho u^2_{ref}} \quad ; \quad C_{fr} = \frac{\tau_r}{\frac{1}{2}\rho u^2_{ref}}$$

In these definitions, τ_c and τ_r are the shear stresses in the chordwise and radial directions, respectively, ρ is the fluid density, and u_{ref} is the reference velocity. The solid lines in Figures 4a and 4b denote the Morris computation and the circles denote the present calculations. The agreement between the two prediction methods is excellent.

$$- m_{13}u - m_{14}w + m_{15} + \theta v$$

$$= m_{10}u \frac{\partial u}{\partial \xi} + m_7 w \frac{\partial u}{\partial \eta} \qquad (25)$$

$$(bt)' - m_4 uw - m_3 w^2 - m_9 u^2 + m_{12}$$

$$+ m_{16}u + m_{13}w - m_{17} + \theta t$$

$$= m_{10}u \frac{\partial w}{\partial \xi} + m_7 w \frac{\partial w}{\partial \eta}$$

$$v' = m_1 u + m_6 w + m_{10} \frac{\partial u}{\partial \xi} + m_7 \frac{\partial w}{\partial \eta}$$

with boundary conditions

$$u = w = v = 0 \quad \text{at} \quad \sigma = 0$$

$$u = 1, \quad w = \frac{w_e}{u_{ref}} \quad \text{at} \quad \sigma = \sigma_\infty \qquad (26)$$

The solution of the first-order equations is obtained using centered finite differences on a net cube and Newton's method. Details of this procedure may be found in Cebeci and Bradshaw (1977).

The calculation of the blade boundary-layer proceeds as follows. Solution marching begins at the hub/leading-edge intersection and moves outward along increasing radii to the tip. Calculations continue in this manner for successively increasing chordwise stations until, finally, the blade trailing edge is reached. Calculations are made over the entire blade surface.

Figure 2 illustrates the calculation procedure in more detail. Calculations at the leading edge begin as laminar at the node denoted (A) in Figure 2 and march radially outward. After completing the leading edge, the solution is obtained at the location of the next chord and first outward radius from the hub, node (B) in Figure 2, using a modified characteristic box method (Bradshaw, et al. (1981)). The characteristic box, which estimates a solution based on the results at the previous chordwise position lying along the same streamline, is traditionally applied only in regions of reverse crossflow. However, this method has been found to be extremely beneficial for propeller blade application near the hub in that it eliminates a complex solution of hub initial conditions.

Once a solution is obtained at location (B), the solution is set at the current chordwise hub position using the initial conditions

$$(f')_H = (f')_B$$

$$(g')_H = \left(\frac{u_e}{u_{ref}}\right)_H \left(g' \frac{u_{ref}}{u_e} - \frac{f' w_e}{u_e}\right) + (f')_B (g')_H$$

Computations continue at increasing radial positions up to the tip using the general box in regions without reverse crossflow and the characteristic box in regions with reverse crossflow. The tip node is always computed using the general box. This general solution pattern is continued along the entire blade.

A transition computation is not incorporated in the present boundary-layer scheme and the location of transition to turbulent flow is an input parameter supplied by the user. The location of transition may be estimated by experimental results, such as flow

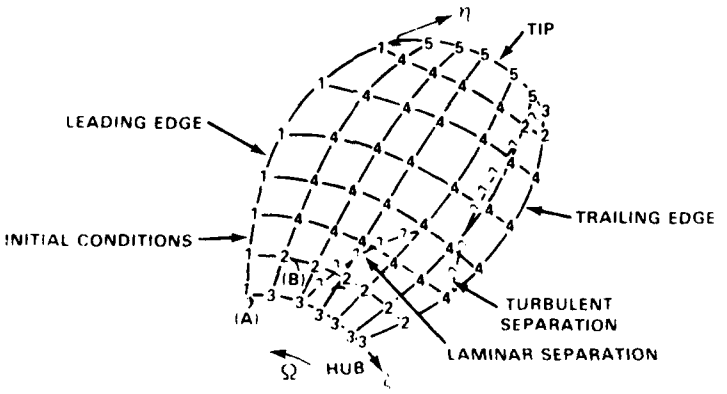

1 LEADING EDGE SOLUTION
2 GENERAL SOLUTION CHARACTERISTIC BOX
3 SOLUTION SET FROM (HUB · 1) OR (TIP 1) SOLUTION
4 GENERAL SOLUTION CHARACTERISTIC OR REGULAR BOX
5 GENERAL SOLUTION REGULAR BOX

Fig 2 Computational Procedure

$$\frac{\partial \frac{w}{u_{ref}}}{\partial n} = \frac{\partial \frac{u_e}{u_{ref}}}{\partial n} G(\xi,\sigma) + \frac{u}{u_{ref}} \frac{\partial w_e}{u_e \partial n} \quad (19)$$

For the special case of $w_e = 0$, as in the rotating disk solution reduces the similarity relations reduce to

$$\frac{u}{u_e} = F(\xi,\sigma)$$

$$\frac{w}{u_{ref}} = \frac{u_e}{u_{ref}} G(\xi,\sigma) \quad (20)$$

$$\frac{\partial \frac{w}{u_{ref}}}{\partial n} = \frac{\partial u_e}{\partial n} \frac{1}{u_{ref}} G(\xi,\sigma)$$

This hub similarity condition is exact for the cases of laminar flow on a rotating segment and a two-dimensional swept wing.

By substituting the general similarity formulations in Equation 19 into the momentum Equations 13 and 14, the derivative quantities $\partial w/\partial n$ are eliminated and marching can proceed in the ξ-direction. Details of the numerical procedure used in the computer code at the hub are given in Section 6 in the numerical analysis. The procedure is self-starting and stable.

5. TURBULENCE MODEL

The governing flow equations presented in Section 4 contain more unknown quantities than equations. A standard procedure in boundary-layer solutions is the introduction of a turbulence model to approximate the Reynolds stress terms $-\overrightarrow{u'v'}$ and $-\overrightarrow{v'w'}$. Various techniques have been developed to handle turbulence modeling, all involving some degree of correlation with experimental data. The zero-equation model is the simplest approach and does not require the solution of any additional differential equations. This method assumes the algebraic specification of both length scale and turbulence energy as explained and used by Cebeci and Smith (1974). The one-equation model solves an equation for the turbulence energy but uses an algebraic specification for the length scale. Although this formulation has been used by Bradshaw, et al. (1976) for thin shear-layers with considerable success, its usage is not wide-spread. Two equation turbulence models, particularly the K-ε model, are experiencing increased popularity. These models are general, but require the solution of two differential equations.

For the present work, the simple zero-equation model of Cebeci and Smith (1974) has been adopted. An eddy-viscosity factor ε_m is defined to relate the Reynolds stresses to the mean velocity profiles by

$$-\overrightarrow{u'v'} = \varepsilon_m \frac{\partial u}{\partial \zeta} \quad \text{and} \quad -\overrightarrow{v'w'} = \varepsilon_m \frac{\partial w}{\partial \zeta} \quad (21)$$

The theoretical boundary layer is divided into an inner region and an outer region with a separate equation defining ε_m in each region. The inner-region formulation is applied from the wall surface to the location in the boundary layer where both inner and outer equations predict the same eddy viscosity. From this location to the edge of the boundary layer, the outer wall formulation is applied.

Eddy viscosity in the inner region is defined as

$$(\varepsilon_m)_i = L^2 \left[\left(\frac{\partial u}{\partial \zeta}\right)^2 + \left(\frac{\partial w}{\partial \zeta}\right)^2 + 2\cos\alpha \left(\frac{\partial u}{\partial \zeta} \frac{\partial w}{\partial \zeta}\right) \right]^{1/2} \quad (22)$$

where L is a mixing length approximation equal to $0.4\zeta \left[1-\exp(1-\zeta/A)\right]$, A is a damping factor equal to $26\nu \left(\frac{\tau_{tw}}{\rho}\right)^{-1/2}$, and τ_{tw} is the turbulent wall shear stress equal to $\mu \left[\left(\frac{\partial u}{\partial \zeta}\right)_w^2 + \left(\frac{\partial w}{\partial \zeta}\right)_w^2 + 2\cos\alpha \left(\frac{\partial u}{\partial \zeta}\right)_w \left(\frac{\partial w}{\partial \zeta}\right)_w\right]^{1/2}$. In the outer region, the eddy viscosity becomes

$$(\varepsilon_m)_o = 0.0168 \left| \int_0^\infty (u_{te} - u_t) d\zeta \right| \gamma_{tr} \quad (23)$$

where u_{te} equals $(u_e^2 + w_e^2 + 2u_e w_e \cos\alpha)^{1/2}$, u_t equals $(u^2 + w^2 + 2uw\cos\alpha)^{1/2}$ and γ_{tr} is an intermittency factor to account for the transition region between viscous and turbulent flow.

6. NUMERICAL ANALYSIS

The governing three-dimensional boundary-layer equations for propeller blades are solved numerically using the Keller (1970) box method. This solution technique may be divided into four steps. Initially, the governing equations are written as a system of first order equations by the introduction of transformed variables. The first order equations are then written in finite difference form using central differences. Newton's method is applied to linearize the difference equations and, finally, the linear system is solved by the block triangular elimination method. New variables u, v, w, t, and v, defined as

$$u' = v = f''$$

$$w' = t = g''$$

$$v' = m_1 u + m_6 w + m_{10} \frac{\partial u}{\partial \zeta} + m_7 \frac{\partial w}{\partial \zeta} \quad (24)$$

are introduced to reduce the ξ- and η-momentum equations to first order. The new system is

$$u' = v$$

$$w' = t$$

$$(bv)' - m_2 u^2 - m_5 uw - m_8 w^2 + m_{11}$$

$$m_9 = s_1 K_1 \csc\alpha \frac{u_e}{u_{ref}}$$

$$m_{10} = \frac{s_1}{h_1}$$

$$m_{11} = m_2 + m_5 \frac{w_e}{u_{ref}} + m_8 \left(\frac{w_e}{u_{ref}}\right)^2$$

$$m_{12} = m_4 \frac{w_e}{u_{ref}} + m_3 \left(\frac{w_e}{u_{ref}}\right)^2 + m_9 + \frac{m_{10}}{u_{ref}} \frac{\partial w_e}{\partial \xi} + \frac{m_7 w_e}{u_{ref}^2} \frac{\partial w_e}{\partial \eta}$$

The new terms m_{13} through m_{17} account for the blade rotation and are defined as

$$m_{13} = \frac{2\Omega s_1}{u_e} \eta_1 \cos\alpha \csc\alpha$$

$$m_{14} = 2\Omega s_1 \eta_1 \csc\alpha \frac{u_{ref}}{u_e}$$

$$m_{15} = m_{13} + m_{14} \frac{w_e}{u_{ref}} \qquad (17)$$

$$m_{16} = \left(\frac{u_e}{u_{ref}}\right)^2 m_{14}$$

$$m_{17} = m_{16} + m_{13} \frac{w_e}{u_{ref}}$$

The boundary conditions for the transformed equations are

$$f = f' = g = g' = 0 \text{ at } \sigma = 0$$

$$f' = 1,\ g' = w_e/u_{ref} \text{ at } \sigma = \sigma_\infty$$

4. INITIAL CONDITIONS

The propeller boundary-layer solution is obtained by marching in the radial direction for chordwise locations increasing from the leading edge to the trailing edge. In this manner, the computation covers the entire blade surface. The solution procedure requires initial velocity profiles along two intersecting planes. These planes are chosen to be the propeller leading edge and hub. Although the marching begins at the radial location termed the hub, the actual flow at hub/blade intersection is too complex to be represented by the boundary-layer analysis. For this paper, the term hub defines a small radial distance outboard of the actual hub/blade intersection where the boundary-layer equations apply. Since the initial conditions are not, in general, known quantities for a given blade geometry, assumptions become necessary to begin the computation. The remainder of this section describes the initial conditions adopted in the present propeller boundary-layer calculation.

For the rotating helical blade, Banks and Gadd (1962) theoretically show that the leading-edge similarity function for the streamwise velocity u satisfies the Blasius equation. This analysis can be extended for application to the propeller blade leading-edge using the equations for the similarity solution of wedge flow. The leading-edge solution of this paper is similar to that adopted by Itoh, et al. (1984) in which the Karman-Pohlhausen profile is used. However, the current method computes the crossflow velocity component w at the leading edge from the η-momentum equation. Itoh, et al. (1984) set these profiles to zero. With the present analysis, the governing equations at the leading edge are

ξ-momentum: $(bf'')' + m_1 ff'' - m_2 (f')^2 + m_{11} = 0$

η-momentum: $(bg'')' + m_1 fg'' + m_{12} = 0$

with the same coefficient terms b, m_1, m_2, m_{11} and m_{12} defined in equations 15 through 17. These equations compute two-dimensional stagnation flow, wedge flow, or flat plate flow at zero incidence depending upon the specified external potential flow velocities at the leading edge. This solution has proven to be both stable and smooth in the boundary-layer calculation at the leading edge and does not require averaging or iterating.

For nonrotating three-dimensional calculations, the second initial condition is specified at locations where the crossflow velocity w equals zero everywhere inside the boundary layer. For the ship hull (Cebeci, et al. (1978)) and the arbitrary wing (Cebeci et al. (1977)), the locations of zero crossflow are the ship keel and the wing root, respectively. For these regions, the η-momentum equation is identically equal to zero and the unknown variables become u, v, and $\frac{\partial w}{\partial \eta}$. That is, for w=0, Equation 14 becomes 0=0. To obtain a solution, a new equation is derived by differentiating the singular η-momentum equation with respect to η. This equation is called the attachment line equation.

For a propeller blade, the solution w=0 everywhere inside the boundary layer is valid only for the blade radius equal to zero and, therefore, should not be used to begin the computation for arbitrary nonzero radii. Itoh, et al. (1984) apply the attachment line solution to the hub of the axial flow pump blade but find it necessary to use an iterative method to obtain a reasonable solution at the hub. In this paper, the method of a similarity solution is adopted at the hub as well as at the leading edge. The similarity relations used at the present time are:

$$\frac{u}{u_e} = F(\xi,\sigma) \ ; \ \frac{\partial}{\partial \eta} \frac{u}{u_e} = 0$$

$$\frac{w}{u_{ref}} = \frac{u_e}{u_{ref}} \frac{w}{u_e} = \frac{u_e}{u_{ref}} G(\xi,\sigma) + \frac{u}{u_{ref}} \frac{w_e}{u_e}$$

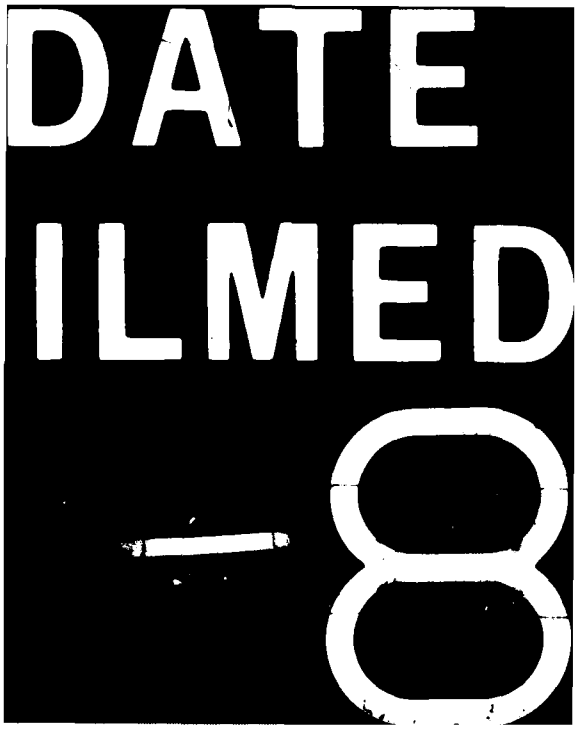
DATE
ILMED
-8